Design Improvement and Performance Analysis of 12Slot-10Pole Permanent Magnet Flux Switching Machine with Field Excitation Coils

E. Sulaiman, *Member, IEEE*, T. Kosaka, *Member, IEEE*, N. Matsui, *Fellow, IEEE*, and M. Z. Ahmad, *Member, IEEE*

Abstract--**Permanent magnet flux switching machine (PMFSM) with additional field excitation coil (FEC) has several attractive features compared to conventional permanent magnet (PM) machines because of its variable flux control capability and robust rotor structure suitable to apply for high speed applications. However, the original machine has a limitation of operating in high current condition due to nonessential magnetic saturation that prevents the machine from extracting the maximum performances. To overcome this problem, some design refinements are conducted by using deterministic optimization method to gain a better performance in the maximum torque and power production. The results simulated by finite element analysis (FEA) show that the machine with the improved design increases by 11.6% of the maximum torque and 16.3% of the maximum power compared to the original design.**

Index Terms--**Permanent magnet flux switching machine (PMFSM), field excitation coil (FEC), permanent magnet (PM), finite element analysis (FEA)**

I. INTRODUCTION

PERMANENT magnet flux switching machines (PMFSMs) have been a popular research topic recently, due to their high power density and robust rotor structure [1]-[2]. With both permanent magnets and armature windings located on the stator and robust single piece rotor similar to that of the switched reluctance machine (SRM), PMFSM have the following advantages compared to conventional PM machines; (1) easy cooling of all active parts in the stator such as armature coil and permanent magnets, and (2) better suitability for high speed applications [3]-[5]. To provide further attractive characteristics, a new structure of 12Slot-10Pole PMFSM with additional field excitation coil has been proposed as shown in Fig. 1 [6]-[8]. Generally, the machine is composed of 12 PMs and 12 FECs distributed uniformly in the midst of each armature coil. The term, "flux switching", is created to describe machines in which the stator tooth flux switches its polarity by following the motion of a salient pole rotor. In this 12Slot-10Pole machine, the PMs and FECs produce six north poles interspersed between six south poles. The three-phase armature coils are accommodated in the 12 slots for each 1/4 stator body periodically. As the rotor rotates, the fluxes generated by PMs and mmf of FECs link with the armature coil alternately. For the rotor rotation through 1/10 of a revolution, the flux linkage of the armature has one periodic cycle and thus, the frequency of back-emf induced in the armature coil becomes ten times of the mechanical rotational frequency. The relation between the mechanical rotation frequency and the electrical frequency for this machine can be expressed as;

$$f_e = Nr \cdot f_m \tag{1}$$

where f_e is the electrical frequency, f_m is the mechanical rotation frequency and N_r is the number of rotor poles respectively.

The cross-sectional view of flux paths caused by both PM and mmf of FEC of the original design is depicted in Fig. 2. Indeed, the presence of FEC makes these types of machines more attractive in terms of modulating the PM flux. The additional FEC gives extra advantage to the machine as the secondary flux source to improve maximum torque and power capabilities due to its variable flux control capability. The proof of principle and some design refinements of this type of machines have also been conducted as in [9]-[10]. This type of machine is classified into hybrid excitation machines which are also getting more popular in recent years [11]-[13].

However, based on initial analysis using FEA, the original PMFSM with FEC designed in Fig. 1 has some drawbacks that prevent the machine from extracting the maximum performances mainly in high current condition. Firstly, this paper provides the design investigations into the original PMFSM with FEC using FEA. The comparison of the torque density characteristics and back-emf waveforms between experimentally obtained in [3] and calculated by FEA is made. Then, the design drawbacks of the original PMFSM with field excitation are discussed. To improve the design drawbacks, some design refinements are conducted using deterministic design approach, resulting in better torque and power performances as well as torque-speed characteristics. In addition, the permanent magnet demagnetization, the rotor mechanical strength, the loss and the efficiency are predicted.

The FEA-based performance predictions of the original PMFSM with FEC are discussed in Section II. The drawbacks of the original machine design are discussed in Section III. Based on finite element analysis (FEA), the method of getting the maximum performances is explained in Section IV. In

E. Sulaiman is with University Tun Hussein Onn Malaysia, Johor, 86400 Malaysia (e-mail: erwan@uthm.edu.my).

addition, the improved design, the PM demagnetization at high temperature, the rotor mechanical strength at high speed, the torque and power versus speed characteristics, the loss and the efficiency are also predicted and discussed in Section V. Finally some conclusions are drawn in Section VI.

II. FEA-BASED PERFORMANCE PREDICTION OF THE ORIGINAL PMFSM WITH FIELD EXCITATION

A. Finite Element Analysis (FEA) Design

FEA design of the original PMFSM with field excitation using commercial package JMAG 10.0 is illustrated in Fig. 3. The number of turns for armature windings (N_a) and excitation winding (N_e) can be calculated as:

$$N_a = \sqrt{\frac{\alpha_a R_a S_a}{4\rho L_{a-ave}}} \text{ and } N_e = \sqrt{\frac{\alpha_e R_e S_e}{12\rho L_{e-ave}}} \quad (2)$$

where, α_a is the filling factor, R_a is the resistance (Ω), S_a is the
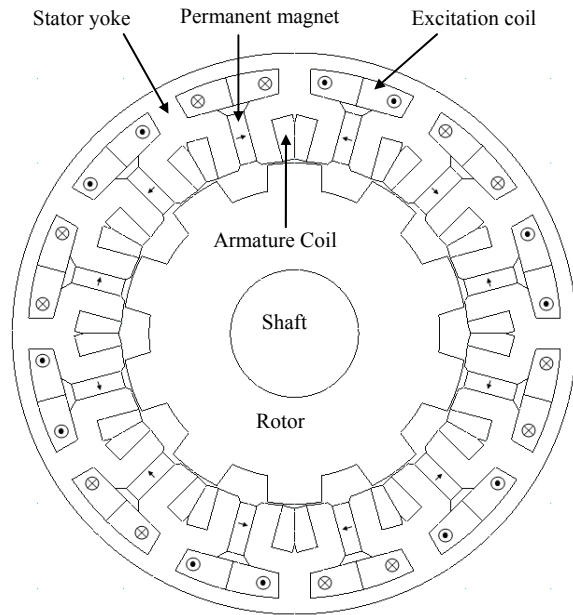

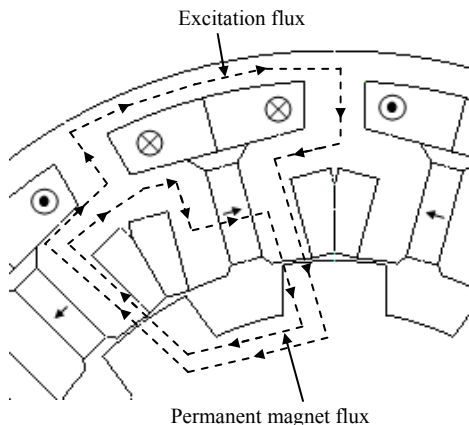Fig. 1. 12Slot-10Pole PMFSM with additional field excitation

Fig. 2. Flux paths of permanent magnet and mmf of excitation coil in 12Slot-10Pole PMFSM with field excitation

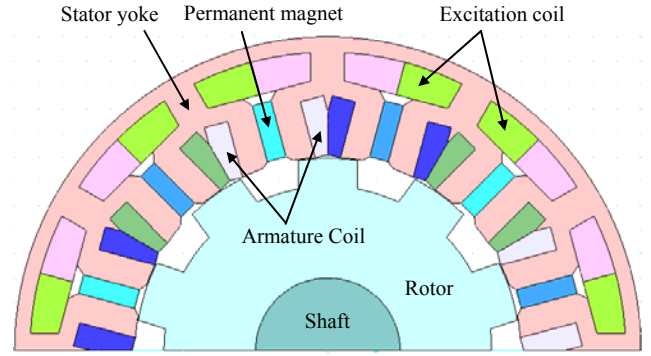area (mm^2), and L_{a-ave} is the average coil length including coil

Fig. 3. FEA design of original PMFSM with field excitation (1/2 model)

end (mm) of armature windings. Similarly, α_e is the filling factor, R_e is the resistance (Ω), S_e is the area (mm^2), and L_{e-ave} is the average coil length including coil end (mm) of excitation winding respectively. In addition, current density of this machine can be calculated using:

$$J_a = \frac{I_a N_a}{\alpha S_a} \text{ and } J_e = \frac{I_e N_e}{\alpha S_e} \quad (3)$$

where, J_a is the current density of armature coil and J_e is the current density of excitation coil respectively. Table I shows the specifications, rated conditions, and the calculated value of N_a, N_e, J_a and J_e.

B. No-Load Analysis

The back-emf during no-load condition at 3000r/min in which the current density of the field excitation is varying from 0 to 15A/mm^2 is shown in Fig. 4. The back-emf shows good agreement between experiment as in [Fig. 6, Ref 3] and FEA but have 8% different at maximum voltage. On the other hand, the torque density versus current density from experimental and FEA at J_e=13A/mm^2 is depicted in Fig. 5. The graph also shows good agreement between experimental and FEA with 6.5% different of torque density at 70A/mm^2. This difference is due to different material used for rotor and stator iron, different permanent magnet, and the analysis using FEA is not considering the iron loss.

TABLE I
SPECIFICATIONS, RATED CONDITIONS AND THE CALCULATED VALUE OF PMFSM WITH FIELD EXCITATION

Armature		Excitation	
α_a	0.5	α_e	0.5
R_a	0.5 Ω	R_e	1.3 Ω
S_a	50.23 mm^2	S_e	77.98 mm^2
ρ	1.69E-08 Ωm	ρ	1.69E-08 Ωm
L_{a-ave}	112.059 mm	L_{e-ave}	123.924 mm
N_a	41 turns	N_e	45 turns
$I_{a\ (Rated)}$	8.5 A	$I_{e\ (Rated)}$	10 A
J_a	13.78 A/mm^2	J_e	11.52 A/mm^2

C. Capability of Original PMFSM with Field Excitation
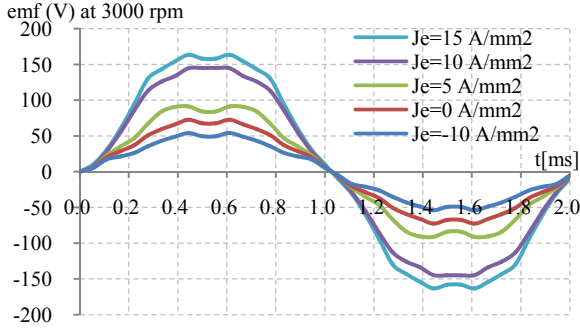

Fig. 4. Back-emf with increasing excitation current density
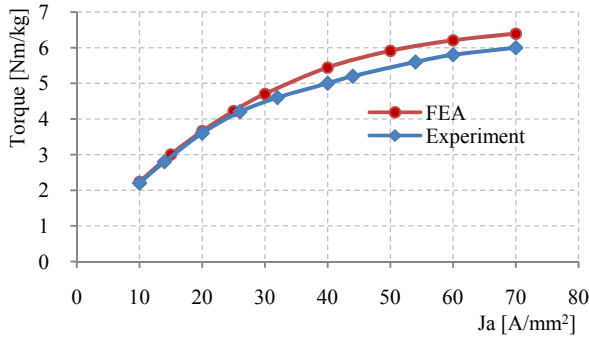

Fig. 5. Torque density comparison between experimental and FEA at $J_e=13A/mm^2$

Design

Since FEA proved the same characteristics as experimental results, current density for each coil can be optimized by estimating maximum torque while increasing excitation current density and minimum power factor while increasing armature current. Fig. 6 shows torque and power factor versus excitation current density at $J_a=15A/mm^2$. Increased the excitation current will increase the torque and power factor, but the torque is limited to its maximum point before gradually decreasing. From the graph, the maximum excitation current density that provide maximum torque is $J_e=21A/mm^2$. Excitation current higher than this value will reduce the torque production but keeping the high power factor. Using the maximum excitation current density noted from Fig. 6, the maximum armature current density that produced maximum torque at minimum power factor can be determined as shown in Fig. 7. It is clear that increasing the armature current density will increased the torque but reduced the power factor. Therefore, maximum armature current density of 27A/mm² is selected at minimum power factor of 0.6. From the maximum current density for armature and field excitation discussed above, the torque density versus armature current density at $J_e=21A/mm^2$ is plotted as shown in Fig. 8. Therefore, the maximum performance of this design can be achieved at the maximum $J_a=27$ A/mm² and $J_e=21$ A/mm² for minimum power factor of 0.6.

III. DRAWBACKS OF ORIGINAL MACHINE DESIGN

According to Fig. 6, the torque reaches its maximum at $J_e=21A/mm^2$ but starts to decrease if J_e is higher than this

value. This phenomenon happens due to the magnetic saturation at stator yoke between armature winding and
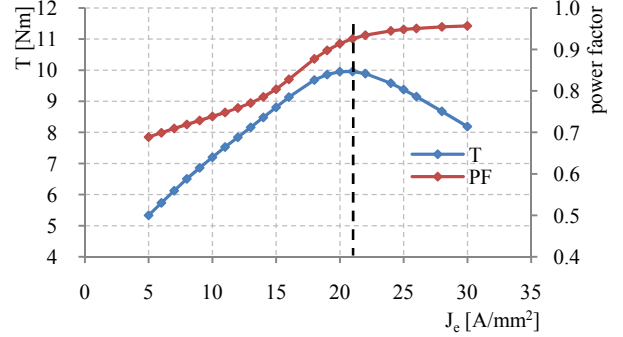

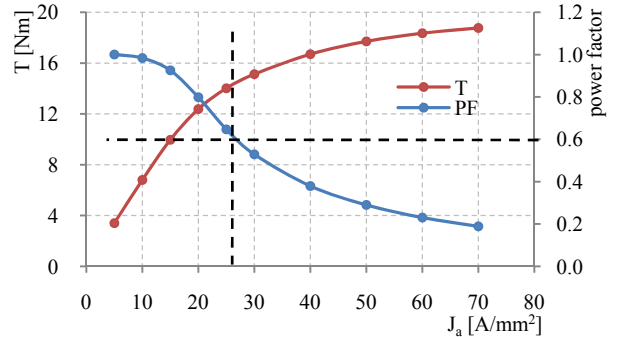Fig. 6. Torque and power factor at $J_a=15A/mm^2$

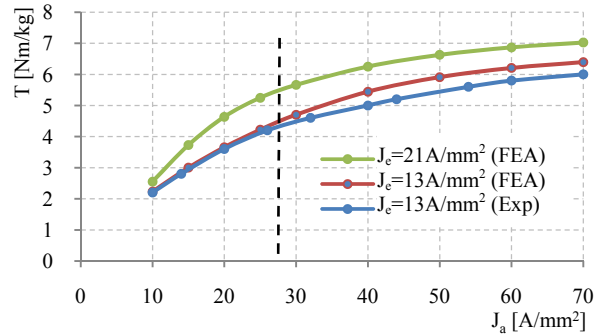Fig. 7. Torque and power factor at $J_e=21$ A/mm²

Fig. 8. Torque density versus armature current density

excitation coil slots marked as A_1 in Fig. 9(b). Compared to the flux path in Fig. 9(a) under less excitation current density with 15A/mm², it is obvious that the magnetic saturation prevents the permanent magnet flux from flowing to the path producing positive torque. As a result, some of permanent magnet fluxes are forced to flow to the rotor side as shown in Fig. 9(b), resulting in negative torque. In other words, higher excitation flux will flow in opposite direction and the permanent magnet fluxes cancel each other at A_2. The remaining permanent magnet flux will flow towards the rotor that produced negative torque hence reducing the total torque. From a design viewpoint, an expansion of the stator yoke width A_1 and A_2 contributes to the conquest of this drawback.
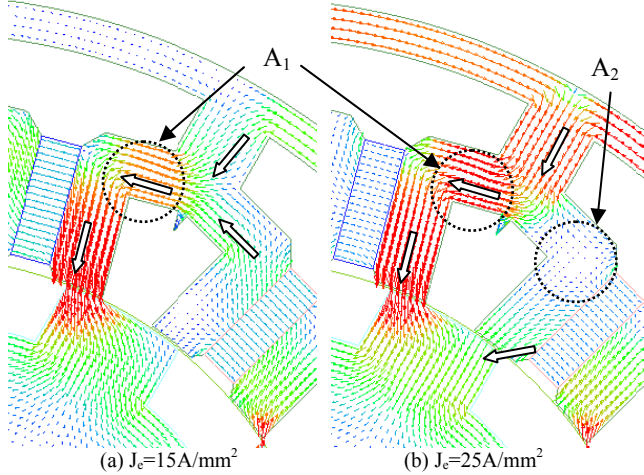
(a) J_e=15A/mm^2 (b) J_e=25A/mm^2

Fig. 9. Comparison between flux vector diagram at low and high excitation current density

IV. FEA BASED DESIGN REFINEMENTS

Commercial FEA package, JMAG-Studio ver.10.0, released by Japan Research Institute (JRI) is used as 2D-FEA solver for this design. The major dimensions of the designed motor are shown in Table II. The permanent magnet material is NEOMAX 35AH whose residual flux density and coercive force at 20C° are 1.2T and 932kA/m, respectively. The electrical steel, 35H-PMA is used for rotor and stator body. To overcome the problem of magnetic saturation between armature winding and excitation coil slots discussed above, and to acquire more high performances, some design parameters are introduced as depicted in Fig. 10. First the necessary coil area S_a is calculated to give optimum integer number of turns of armature coil N_a. Then, the maximum gap between armature coil-excitation coil and armature coil-permanent magnets is redesign to get maximum torque while keeping the necessary power factor. This is followed by designing the rotor diameter, salient pole arc and depth of teeth to get its maximum performance. Finally the curve shape at every coil edge is designed to allow flux to flow smoothly. The method of finding the maximum performance of this machine is by adjusting parameters D_1 to D_7 by trial and error with keeping the same volume of permanent magnets and air gap length.

V. IMPROVED DESIGN AND RESULTS

A. Improved Design

The comparison between original and improved design of the machine is illustrates in Fig. 11. It is clear that the improved design has much gap between the armature and excitation coil allowing more fluxes to flow. Fig. 12 illustrates the flux path of the improved design for J_e=20 A/mm^2 and J_e=30 A/mm^2. Since the stator yoke width B_1 between the armature and the excitation coils is expanded, the magnetic saturation caused by higher excitation current is relaxed. Thus, the improved design maintains the same torque for both

current density conditions and enables to extract higher power factor without any reduction of the torque at high excitation current density. Furthermore, the torque and power factor versus excitation current density at armature current density J_a=15 A/mm^2 are shown in Fig. 13. The torque is increased 11.65% more than original design until J_e=27 A/mm^2 and keep constant after this value. The graph also shows that power factor is increased and keeps high at high excitation current density. This condition proves that the improved design can increase the torque and power factor without reducing the torque at high excitation current density.

B. Magnet Demagnetization at High Temperature

Selection of permanent magnet materials is also important to avoid permanent magnet demagnetization if the machine is exposed in high temperature condition. The demagnetization of permanent magnet is calculated as:

$$\%D = \sum \frac{A_n(B_n < B_{CP})}{\sum A_n} \tag{4}$$

where, A is area of the permanent magnet (mm^2), B is the magnetic flux density (T), n is number of element, and CP is the knee point of the permanent magnet according to BH curve. The calculated value by FEA of each element shows that this magnet has 0% demagnetization at high temperature as high as 180°C.
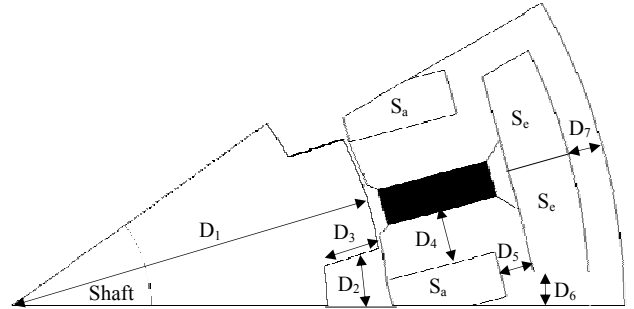

Fig. 10. Comparison between flux vector diagram at low and high excitation current density

TABLE II
MAIN DIMENSIONS OF THE DESIGNED MOTOR

External diameter	130 mm
Inner diameter	80 mm
Air gap length	0.2 mm
Active length	30 mm
Stator iron mass	1.04 kg
Rotor iron mass	0.88 kg
PM : NEOMAX-35AH	1.2 T
PM volume	17.2 cm3 – 131 g
Phases copper mass	0.3 kg
Excitation copper mass	0.34 kg
Total weight	2.671kg

C. Rotor Mechanical Strength at High Speed

The mechanical stress prediction of rotor structure at high speed 20,000r/min is calculated by centrifugal force analysis based on 2D-FEA. Fig. 14 illustrates the principal stress distributions of the rotor core for the finally designed machine. The highest stress can be found at a point highlighted in circle. It shows that the maximum principal stress at 20,000r/min reaches 19.7MPa which is much smaller than 300MPa being allowable as the maximum principal stress in conventional electromagnetic steel. This is a great advantage of the designed machine that makes it applicable for high-speed application such as hybrid electric vehicles.
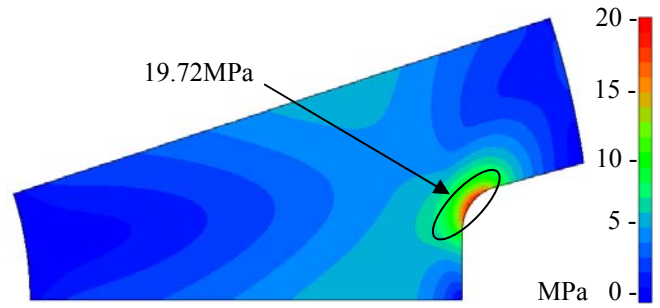

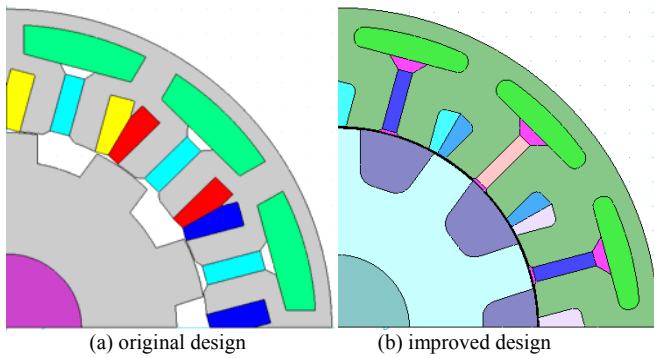Fig. 14. Principal stress distribution of rotor at 20,000r/min
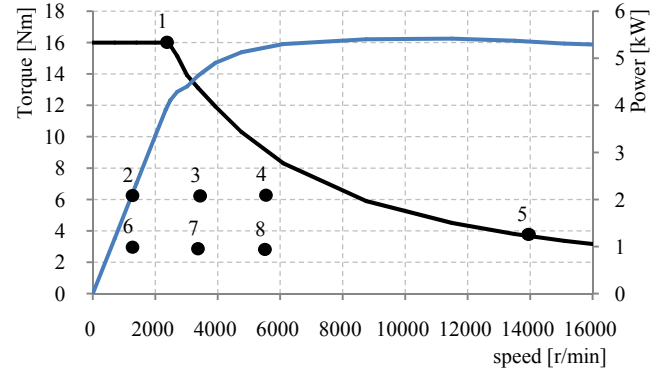

Fig. 15. Torque and power versus speed characteristics

Fig. 11. Original and improved design

(a) original design (b) improved design

Fig. 16. Loss analysis and motor efficiency at frequent operating points
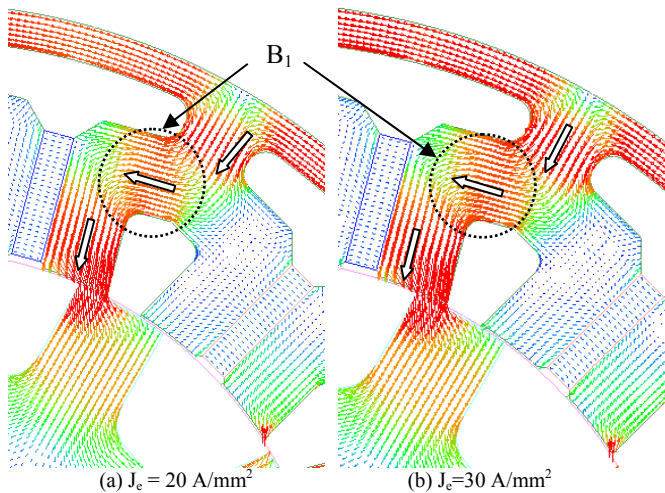

(a) $J_e = 20$ A/mm^2 (b) $J_e=30$ A/mm^2
Fig. 12. Comparison between flux vector diagram at low and high excitation current density for the final designed machine

TABLE III
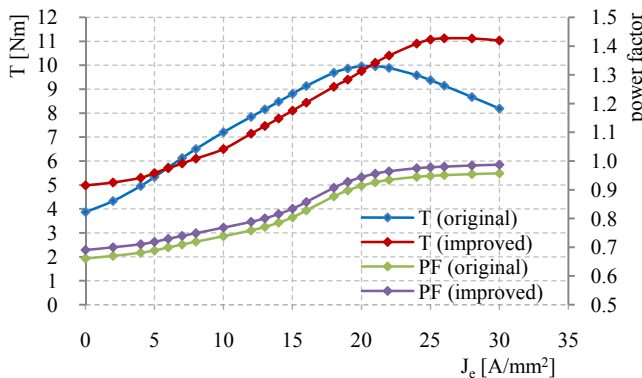PERFORMANCE OF PMFSM WITH FIELD EXCITATION

	Original Design	Improved Design	
J_a(A/mm^2)	15	15	30
J_{e-max}(A/mm^2)	21	27	30
T (Nm)	9.96	11.12	16.03
T (Nm/kg)	3.74	4.16	6.00
PF	0.92	0.98	0.63
P (kW)	2.83	3.29	5.41
Rotor Mechanical Strength (MPa)			19.72
PM Demagnetization (180°C)			0.0%
Motor Efficiency			> 90%

Figure 13. Torque and power factor at J_a=15A/mm^2

D. Torque and Power versus Speed Characteristics

The torque and power versus speed curves of the finally designed machine is plotted in Fig. 15 where the current density is limited to the maximum of 30A/mm^2 for each coils.

In the figure, the solid black line depicts the maximum torque curve for operating speed of the final designed machine. At base speed 2,274r/min, the torque obtained is 16.03Nm as the maximum and the corresponding power reaches 4.25kW with the power factor of 0.63. The maximum power 5.41kW is achieved at high speed 10,000r/min. In addition, the average power of 4.92kW is achieved between 4,000 - 6,000r/min. Finally, the maximum torque density and maximum power density obtained are 5.99Nm/kg and 2.03kW/kg, respectively.

E. Motor Loss and Efficiency

The motor loss and efficiency are calculated by finite element analysis considering copper losses in armature coil and field excitation coil, and iron losses in all laminated cores. Fig. 15 also demonstrates specific operating points at maximum torque, maximum power, and frequent operating point under light load noted as No. 1 to No. 8. Meanwhile, the detailed loss analysis and motor efficiency of the designed machine are summarized in Fig. 16. At high torque operating points No.1, the motor efficiency is 94.1% although it has high copper loss. At high speed operating point No. 5, the efficiency is 90.4%, degraded due to increase in iron loss. Furthermore, at operating point No. 2 to No. 4 and No. 6 to No. 8 under low load conditions, the proposed machine achieves relatively high efficiency approximately more than 92%. As a result, it is concluded that the proposed machine can work for specific operating points with high efficiency as much as 90% to 97%. The overall performances of the proposed machine based on finite element analysis are summarized in Table III.

VI. Conclusion

This paper has presented the design improvement and performance analysis of permanent magnet flux switching machine with field excitation. The research goal to get the maximum performance has been achieved by improving the flux path to avoid flux saturation and by increasing torque and output power. This machine can also be employed for motor with robust condition due to its high mechanical strength, zero magnet demagnetization at high thermal environment as well as high revolution speed such as hybrid electric vehicle.

VII. References

[1] Z. Q. Zhu, Y. Pang, D. Howe, S. Iwasaki, R. Deodhar, and A. Pride, "Analysis of electromagnetic performance of flux-switching PM machine by nonlinear adaptive lumped parameter magnetic circuit model," *IEEE Trans. Magnetics*, vol. 41, no.11 pp. 4277–4287, Nov. 2005.

[2] E. Hoang, A. H. Ben-Ahmed, and J. Lucidarme, "Switching flux permanent magnet polyphased synchronous machines," in *Proc. 1997 7th European Conf. on Power Electronics and Appl.*, vol. 3, pp. 903-908.

[3] J. T. Chen, Z. Q. Zhu, and D. Howe, "Stator and Rotor Pole Combinations for Multi-Tooth Flux-Switching Permanent-Magnet Brushless AC Machines", IEEE Trans. Magnetics, vol. 44, no. 12, pp. 4659-4667, Dec. 2008.

[4] E. Ilhan, B. L. J. Gysen, J. J. H. Paulides, and E. A. Lomonova, "Analytical Hybrid Model for Flux Switching Permanent Magnet Machines" IEEE Trans. Magnetics, vol. 46, no. 6, pp. 1762-1765, June 2010.

[5] Z. Q. Zhu, and J. T. Chen, "Advanced Flux-Switching Permanent Magnet Brushless Machines," *IEEE Trans. Magnetics*, vol. 46, no.6 pp. 1447–1453, June 2010.

[6] E. Hoang, M. Lecrivain, and M. Gabsi, "A new structure of a switching flux synchronous polyphased machine with hybrid excitation," in *Proc. 2007 European Conf. on Power Electronics and Applications*, pp. 1-8.

[7] E. Hoang, S. Hlioui, M. Lecrivain, and M. Gabsi, "Experimental comparison of lamination material case switching flux synchronous machine with hybrid excitation," in *Proc. 2009 European Conf. on Power Electronics and Applications*, pp. 1-7.

[8] E. Sulaiman, Y. Tsujimori, T. Kosaka and N. Matsui, "Design of 12-slot 10-pole permanent magnet flux switching machine with hybrid excitation for hybrid electric vehicle," in *Proc. 2010 The 5th IET Int. Conf. on Power Electronics, Machine and Drives*, pp. 1-5.

[9] E. Sulaiman, T. Kosaka, and N. Matsui, "Design and performance of 6-slot 5-pole permanent magnet flux switching machine with hybrid excitation for hybrid electric vehicle applications," in *Proc. 2010 Int. Power Electronics Conf.*, pp. 1962-1968.

[10] W. Hua, M. Cheng, and G. Zhang, "A Novel Hybrid Excitation Flux-Switching Motor for Hybrid Vehicles," IEEE Trans. Magnetics, vol. 45, no. 10, pp. 4728-4731, Oct. 2009.

[11] T. Kosaka, M. Sridharbabu, M. Yamamoto, and N. Matsui, "Design studies of hybrid excitation motor for main spindle drive in machine tools", *IEEE Trans. Industrial Electronics*, vol. 57, no. 11, pp. 3807–3813, Nov. 2010.

[12] E. Sulaiman, T. Kosaka, and N. Matsui, "FEA-based design and parameter optimization study of 6-slot 5-pole PMFSM with field excitation for hybrid electric vehicle," in *Proc. 2010 Int. Conf. on Power and Energy*, pp. 206-211.

[13] I. Ozawa, T. Kosaka and N. Matsui, "Less Rare-Earth Magnet-High Power Density Hybrid Excitation Motor Designed for Hybrid Electric Vehicle Drives", in *Proc. 2009 European Conf. on Power Electronics and Applications*, pp. 1-10.